An Ultra-low-power Power Management Circuit with Output Bootstrapping and Reverse Leakage Reduction Function for RF Energy Harvesting

Zizhen Zeng[#1], Shanpu Shen[$], Bo Wang[*], Johan J. Estrada-López[#], Ross Murch[$], Edgar Sánchez-Sinencio[#]

[#]ECE Dept., Texas A&M University, USA

[$]ECE Dept., Hong Kong University of Science and Technology, Hong Kong SAR

[*]Division of ICT, CSE, Hamad Bin Khalifa University, Qatar

[1]zzzeng@tamu.edu

***Abstract*— The reverse leakage current in the rectifier is a key challenge in the design of RF energy harvesting (RF-EH) systems, especially in harvesting modulated RF signals from WLAN band. In this paper, we propose a dual-band energy harvesting system operating at GSM-900 (900 MHz) and WLAN (2.4 GHz) bands. To harvest the RF energy from the WLAN band more efficiently, an event-triggered 1:2 parallel-series switched-capacitor (SC) converter is proposed to reduce the reverse leakage current. Meanwhile, this SC converter can provide an output voltage bootstrapping function while maintaining an ultra-low-power consumption down to 28 nW by asynchronous control. The power management unit (PMU) with the rectifier is fully integrated in a CMOS 130-nm process. Measurement results have shown the PMU can boost up the output voltage by 1.73× with an input voltage as low as 0.2 V. When harvesting the modulated waveform, the RF-EH system output ripple is decreased by 6×, and reverse leakage current reduction is over 2500× compared to the direct connection condition.**

***Keywords*— Asynchronous control, bootstrapping, power management, RF energy harvesting, leakage reduction, switched capacitor converter, WLAN**

I. Introduction

Radio frequency energy harvesting (RF-EH) technology is a promising technology for Internet-of-Things (IoT) applications [1]. However, one challenge of RF energy harvesting is the limited RF-to-DC efficiency, especially for the low input RF power range. To improve the efficiency in the low input power range, low threshold devices or threshold compensated topologies are commonly adopted to reduce the forward voltage loss while sacrificing the diode reverse current clamping abilities [2], [3]. To further improve its efficiency, the input RF waveform optimized for wireless power transfer has been studied recently [4], [5]. It is found that the amplitude modulated waveform can improve the rectifier efficiency when the waveform is near its peak value. However, when the waveform stays in the valley region, the undesired diode reverse leakage will discharge the energy-storage capacitor loading, which causes the output voltage drop and degrades the overall performance. A larger capacitor would be required to limit this undesired voltage drop. What's worse, if the input RF power is weak or even zero periodically, the output voltage of the rectifier will decrease abruptly due to this leakage current. To solve this issue, in the conventional RF-EH based battery charging systems as shown in Fig. 1(a), a switch controlled by the power management unit (PMU) is inserted to reduce the reverse leakage current. However, the power consumption of PMU is high as micro-watts [6], [7] and it needs to monitor the direction of current flow continuously. In this paper, a novel switched-capacitor (SC) converter is proposed at the output of the rectifier as shown in Fig. 1(b). This converter can boost up the output voltage of the RF-EH system for better energy storage. More importantly, it blocks the leakage current from the main battery to the rectifier. To keep the control power overhead to a minimum level, an asynchronous control scheme is proposed to replace power-hungry clocking elements. As a result, the voltage conversion efficiency is significantly improved in such low-frequency operations with minimized switching loss and minimized consumed power. When the RF power is weak or zero, the PMU automatically stays in the idle mode until the RF power is high enough.

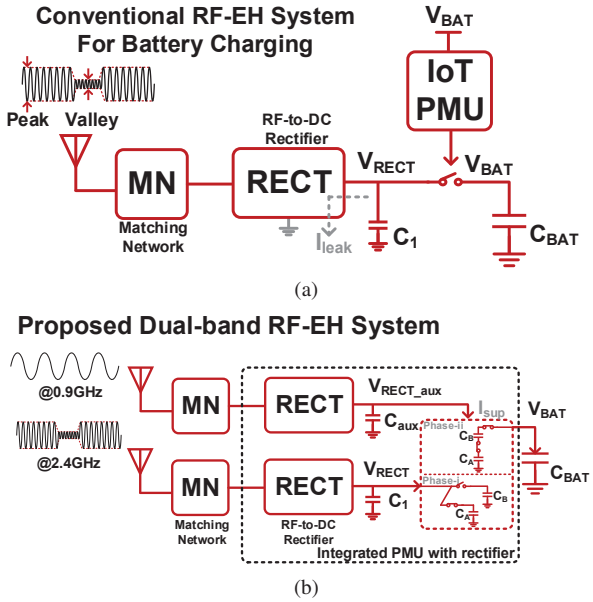

Fig. 1. (a) Conventional RF-EH PMU and (b) our proposed RF-EH PMU.

Our proposed RF-EH system operates at GSM-900 (900

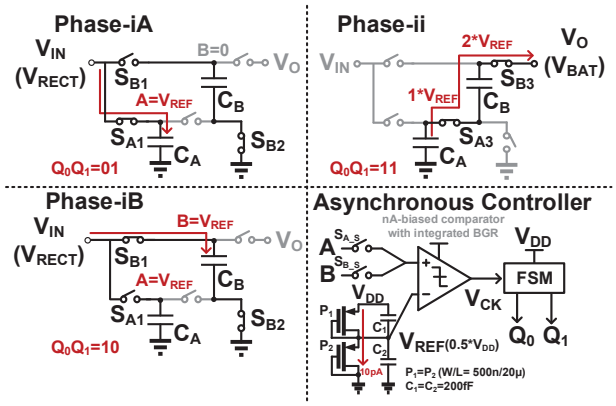

Fig. 2. Asynchronous-controlled 1:2 parallel-series SC converter principles.

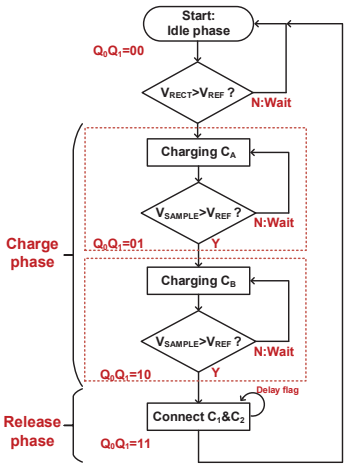

Fig. 3. Event-triggered PMU FSM diagram.

MHz) and WLAN (2.4 GHz) bands. As shown in Fig. 1(b), a dual-port structure is adopted so that one antenna port harvests RF energy from WLAN and the other antenna port harvests RF energy from GSM-900. Particularly, the RF waveform from WLAN is highly related to user behaviors with high PAPR, which will cause current leakage and degraded performance. Therefore, we propose a novel PMU architecture with output voltage bootstrapping and reverse leakage current reduction function to efficiently harvest the WLAN RF energy.

This paper is organized as follows: Section II discusses the design details of the proposed power management system. Section III shows the measurement results and literature comparison. Section IV concludes the whole work.

II. Design of the Proposed RF-EH System

The RF-EH system includes rectifiers with an off-chip matching network and an SC converter PMU. The rectifier topology is a two-stage Dickson rectifier employing native transistors [8]. The typical threshold voltage is simulated as 125 mV. As shown in Fig. 1(b), the PMU supply V_{DD} is powered up by another rectifier optimized for GSM-900 band. The PMU input V_{IN} is connected to the output of

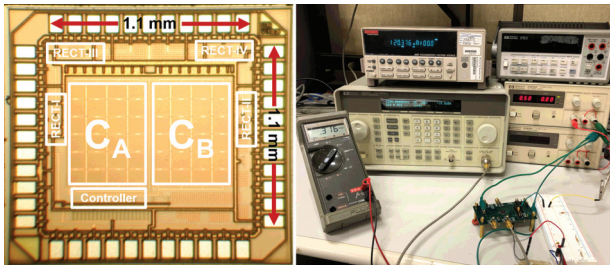

Fig. 4. Die micrograph and measurement test-bench photograph.

2.4 GHz rectifier. The PMU output V_O is connected to a capacitor loading that serves as a battery to store the harvested energy. The PMU can also be self-powered up in a single-port system with single band operations. In this case, the PMU is configured as a 1:1 SC converter by simply connecting the V_{DD} to the V_O directly in the self-sustain mode. Nevertheless, the dual-band operations can make full advantage of the ambient RF power from different bands, and the dual-port structure can achieve optimization for each band separately. The PMU is powered up by the harvested GSM-900 power through the other port. And because this PMU only consumes power in nano-watts, this harvested power from GSM-900 band can be used to power up the IoT sensor loading simultaneously.

A. Asynchronous 1:2 Parallel-Series SC Converter.

Fig. 2 shows the working principles of the 1:2 parallel-series SC converter PMU. In conventional designs, the switches are driven by the clock signals which requires dynamic power in the level of μW. To accommodate with the RF-EH scenarios, a novel asynchronous SC converter is proposed. An nA-biased (through an ultra-low-power band-gap reference (BGR) [9]) comparator continuously monitors the voltage of the capacitor bank. Its output V_{CK} invokes the internal finite-state-machine (FSM). Firstly, in phase-iA, the switch S_{A1} connects the bank capacitor C_A to the rectifier and the voltage of C_A is monitored by the comparator through the switch S_{A_S}. The rectifier will charge up the internal 0.5 nF capacitor C_A to the internal reference voltage V_{REF} ($0.5\times V_{DD}$). And then in phase-iB, another capacitor C_B is charged up successively. When both capacitors are fully charged up to V_{REF}, the system moves to the release phase. C_A and C_B are connected in series to boost up the output voltage. In the steady stage, the final output voltage is ideally $2\times V_{REF}$. The switches S_{A1}, S_{B1} and S_{B3} between the rectifier and the battery will not be turned on simultaneously. Therefore, the leakage current from the battery to the rectifier is significantly reduced. The V_{REF} can be replaced with other voltage reference, and the internal voltage divider is adopted here to make sure the final output voltage can not exceed V_{DD} for voltage protection.

B. Event-triggered PMU Finite-State-Machine (FSM)

The FSM of the PMU system is illustrated in Fig. 3. Notice the modular design of the SC topology, which means that if a higher conversion ratio is required, the system could

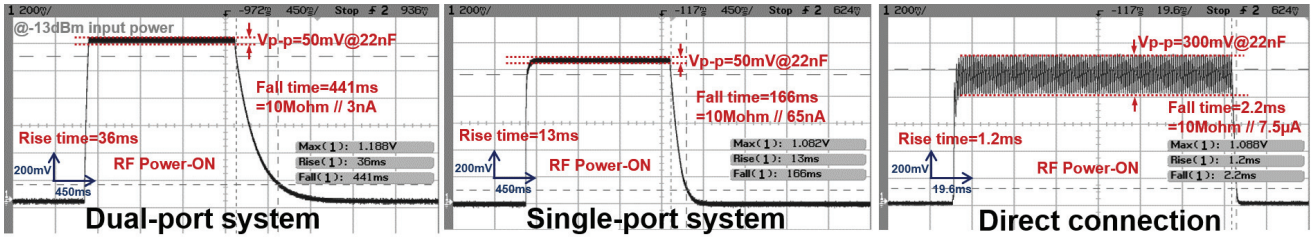

Fig. 5. Cold start-up results under AM modulated power. (with a 10-MΩ probe)

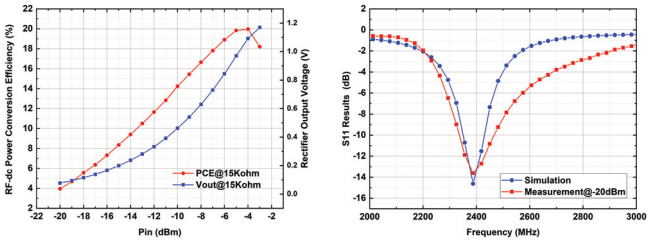

(a) (b)

Fig. 6. (a) RF-DC PCE and (b) S_{11} measurement with simulation results.

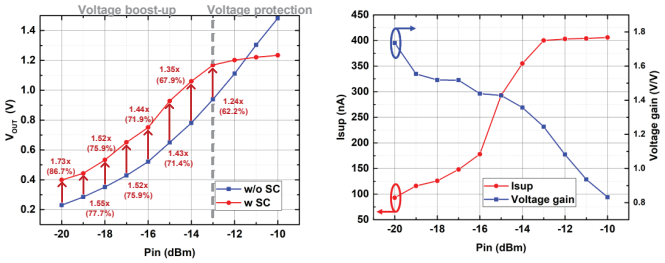

(a) (b)

Fig. 7. (a) RF-EH and (b) SC converter performance. (with a 10-MΩ probe)

be expanded to 1:n configuration for higher output voltage. In the release phase, the energy stored in the capacitor is delivered to the output. After the charge is released, the system is back to the idle phase for the next trigger signal. The PMU self-oscillating frequency is dependent on the low modulation frequency (1 kHz in this work) of the input RF waveform because the output of the RF-DC rectifier is changed abruptly along with the dynamic input power. In this approach, if the ambient RF power is too weak or suddenly disappears, the system can maintain in the idle phase and the connection between rectifier and the loading is cut-off to avoid reserve leakage current. The system can process the charge delivery once the capacitor voltage exceeds V_{REF} again.

III. Measurement Results

The PMU with rectifier is fabricated in CMOS 130-nm process and the matching network is designed with discrete components. Fig. 4 shows the chip micrograph (1.1mm×1.1mm) with the test bench. To imitate the modulated waveform, a 2.4 GHz amplitude modulation (AM) waveform at 1 kHz is injected from the RF signal generator for simplicity. In the dual-port PMU with WLAN rectifier measurement, an external DC power supply is used as the PMU supply voltage to characterize the system performance under different V_{DD} before the final integration.

Fig. 5 shows the transient output waveform of three different cases under the same input power, including the dual-port system (V_{DD} fed separately), single-port system (V_{DD} fed by the output V_{BAT}), and the direct connection (rectifier connected to V_{BAT} directly without the SC converter). The ripple reduction of our purposed system is 6× compared to the direct connection under the same 22 nF loading capacitor. When the RF power is off, the falling time compared to the generic topology, is 200× and 75× respectively. To characterize the reverse leakage current reduction performance, a constant current source is used to represent the average leakage current. The equivalent average leakage current is 3 nA and 65 nA respectively compared to 7.5 μA in the direct connection, which is reduced by 2500× and 115×. The error introduced by the 10 MΩ probe is also included in the calculation. The rise time is measured as 36 ms (30×) and 13 ms (11×) compared to its leakage reduction performance.

Fig. 6 shows the RF-DC rectifier power conversion efficiency (PCE) performance under 2.4 GHz. The rectifier working range is from −20 dBm to −2 dBm with a sensitivity point at −20 dBm for 4% PCE and peak PCE of 20% at −4 dBm. When the input power is larger than −4 dBm, the PCE

Table 1. Literature review and comparison.

Work	TMTT-19 [6]	JSSC-19 [2]	IMS-17 [7]	**This work**
Process	Discrete	65 nm	180 nm	**130 nm**
Frequency	2.45 GHz	2.45 GHz	400 MHz	**2.4 GHz**
Rectifier sensitivity	2%@ −20 dBm	2%@ −17 dBm	10%@ −13 dBm	**4%@ −20 dBm**
Rectifier peak PCE	38%@ 13 dBm	48.3%@ −3 dBm	59% @ −8 dBm	**20%@ −4 dBm**
PMU type	Switched-L	Switched-L	SC	**Asyn. SC**
Achieved voltage gain	1.3	NA	<1 (step-down)	**1.73**
PMU working range	NA	>−19 dBm	−12 to −1 dBm	**>−20 dBm**
PMU consumed power	>47 μW*	>1 μW	35 μW*	**28 - 405 nW**
PMU integration	No	No	Yes	**Yes**
Start-up voltage	NA	0.38 V	1.2 V	**0.2 V**
PMU V_{DD}	>3.0 V	NA	>1.2 V	**0.3-1.0 V**
RF-EH V_{OUT}	0-14 V (w/o PMU)	>2.2 V (w PMU)	1.2 V (regulated)	**0.4-1.2 V (w SC)**

drops down because the 1.2 V Electrostatic discharge (ESD) voltage clamps the output voltage at 1.2 V for protection. Our design is better in a low power range than other designs even using a more advanced process. The measured S_{11} result [Fig. 6(b)] matches with the simulation as well. The S_{11} simulation model includes the rectifier linear model, transmission line and package model.

Fig. 7 shows the WLAN RF-EH system output voltage under capacitor loading with and without the SC converter. The maximum voltage boost gain is measured as 1.73× even in very low input voltage around 0.2 V at the minimum input power −20 dBm (86.7% compared to the ideal conversion gain). When input power is higher than −13 dBm, the system is in voltage protection mode because of the ESD protection. And the SC converter protects the battery from overcharge in this mode. The system total power consumption is measured from 28 nW to 405 nW with V_{DD} from 0.3 to 1.0 V, which includes all the circuit blocks.

Compared to other designs listed in Table 1, our RF-EH system can provide better performance especially in the low input power range with a fully integrated and low-cost solution. Our proposed SC converter achieves the minimum power consumption down to 28 nW. Its capability of blocking the reverse leakage current and meanwhile, boosting up the output voltage is experimentally verified. Compared to the other PMU that requires larger power consumption, the proposed design can extend its working range to the minimum input power as −20 dBm with an rectifier output of 0.2 V.

IV. Conclusion

In this work, a dual-band RF-EH system is presented. Particularly, to harvest the RF energy from 2.4 GHz WLAN band more efficiently, a novel asynchronous SC converter is proposed to perform output voltage bootstrapping and reverse leakage current reduction. The whole system can be self-started up when the input power is larger than −20 dBm with the minimum power consumption 28 nW. Our future work is to achieve co-design the PMU with the multi-port antenna.

Acknowledgment

This work was partially supported by Texas Instruments, Silicon Labs and NPRP grant NPRP11S-0104-180192 from the Qatar National Research Fund (a member of Qatar Foundation).

References

[1] S. Shen *et al.*, "An ambient RF energy harvesting system where the number of antenna ports is dependent on frequency," *IEEE Transactions on Microwave Theory and Techniques*, vol. 67, no. 9, pp. 3821–3832, Sep. 2019.

[2] P. Xu *et al.*, "Analysis, modeling, and design of a 2.45-GHz RF energy harvester for SWIPT IoT smart sensors," *IEEE Journal of Solid-State Circuits*, vol. 54, no. 10, pp. 2717–2729, Oct 2019.

[3] Z. Zeng *et al.*, "Design of sub-gigahertz reconfigurable RF energy harvester from -22 to 4 dBm with 99.8% peak MPPT power efficiency," *IEEE Journal of Solid-State Circuits*, vol. 54, no. 9, pp. 2601–2613, Sep. 2019.

[4] N. Ayir *et al.*, "Experimenting waveforms and efficiency in RF power transfer," *2019 IEEE MTT-S International Microwave Symposium (IMS)*, pp. 1140–1143, June 2019.

[5] B. Clerckx *et al.*, "Fundamentals of wireless information and power transfer: From RF energy harvester models to signal and system designs," *IEEE Journal on Selected Areas in Communications*, vol. 37, no. 1, pp. 4–33, Jan 2019.

[6] S. Fan *et al.*, "A 2.45-GHz rectifier-booster regulator with impedance matching converters for wireless energy harvesting," *IEEE Transactions on Microwave Theory and Techniques*, vol. 67, no. 9, pp. 3833–3843, Sep. 2019.

[7] S. Lin *et al.*, "A high-efficiency power management IC with power-aware multi-path rectifier for wide-range RF energy harvesting," *2017 IEEE MTT-S International Microwave Symposium (IMS)*, pp. 304–306, June 2017.

[8] Z. Zeng *et al.*, "A reconfigurable rectifier with optimal loading point determination for RF energy harvesting from -22 dbm to -2 dbm," *IEEE Transactions on Circuits and Systems II: Express Briefs*, pp. 1–1, 2019.

[9] M. Seok *et al.*, "A portable 2-transistor picowatt temperature-compensated voltage reference operating at 0.5 V," *IEEE Journal of Solid-State Circuits*, vol. 47, no. 10, pp. 2534–2545, Oct 2012.